ISSN 1674-1056
http://cpb.iphy.ac.cn
http://iopscience.iop.org/cpb
中国物理 B
Chinese Physics
中国物理 Chinese Physics B

Multi-carrier transport in $ZrTe_5$ film

Fangdong Tang(汤方栋), Peipei Wang(王培培), Peng Wang(王鹏), Yuan Gan(甘远), Le Wang(王乐), Wei Zhang(张威), Liyuan Zhang(张立源)

Citation: Chin. Phys. B . 2018, 27(8): 087307. **doi:** 10.1088/1674-1056/27/8/087307

Journal homepage: http://cpb.iphy.ac.cn; http://iopscience.iop.org/cpb

What follows is a list of articles you may be interested in

Topological transport in Dirac electronic systems: A concise review

Hua-Ding Song(宋化鼎), Dian Sheng(盛典), An-Qi Wang(王安琦), Jin-Guang Li(李金光), Da-Peng Yu(俞大鹏), Zhi-Min Liao(廖志敏)

Chin. Phys. B . 2017, 26(3): 037301. **doi:** 10.1088/1674-1056/26/3/037301

AlO_x/LiF composite protection layer for Cr-doped $(Bi, Sb)_2Te_3$ quantum anomalous Hall films

Yunbo Ou(欧云波), Yang Feng(冯洋), Xiao Feng(冯硝), Zhenqi Hao(郝镇齐), Liguo Zhang(张立果), Chang Liu(刘畅), Yayu Wang(王亚愚), Ke He(何珂), Xucun Ma(马旭村), Qikun Xue(薛其坤)

Chin. Phys. B . 2016, 25(8): 087307. **doi:** 10.1088/1674-1056/25/8/087307

Electron states scattering off line edges on the surface of topological insulator

Shao Huai-Hua, Liu Yi-Man, Zhou Xiao-Ying, Zhou Guang-Hui

Chin. Phys. B . 2014, 23(10): 0107304. **doi:** 10.1088/1674-1056/23/10/107304

Organic magnetoresistance based on hopping theory

Yang Fu-Jiang, Xie Shi-Jie

Chin. Phys. B . 2014, 23(9): 097306. **doi:** 10.1088/1674-1056/23/9/097306

Confined states and spin polarization on a topological insulator thin film modulated by an electric potential

Liu Yi-Man, Shao Huai-Hua, Zhou Xiao-Ying, Zhou Guang-Hui

Chin. Phys. B . 2013, 22(7): 077310. **doi:** 10.1088/1674-1056/22/7/077310

Multi-carrier transport in $ZrTe_5$ film*

Fangdong Tang(汤方栋)[1,2], Peipei Wang(王培培)[2], Peng Wang(王鹏)[2], Yuan Gan(甘远)[2], Le Wang(王乐)[1,†], Wei Zhang(张威)[1], and Liyuan Zhang(张立源)[2]

[1] *Department of Physics and Beijing Key Laboratory of Optoelectronic Functional Natual Materials & Micro-nano Devices, Renmin University of China, Beijing* 100872, *China*

[2] *Department of Physics, Southern University of Science and Technology, Shenzhen* 518055, *China*

(Received 10 April 2018; revised manuscript received 1 June 2018; published online 10 July 2018)

Single-layered zirconium pentatelluride ($ZrTe_5$) has been predicted to be a large-gap two-dimensional (2D) topological insulator, which has attracted particular attention in topological phase transitions and potential device applications. Herein, we investigated the transport properties in $ZrTe_5$ films as a function of thickness, ranging from a few nm to several hundred nm. We determined that the temperature of the resistivity anomaly peak (T_p) tends to increase as the thickness decreases. Moreover, at a critical thickness of ~ 40 nm, the dominating carriers in the films change from n-type to p-type. A comprehensive investigation of Shubnikov–de Hass (SdH) oscillations and Hall resistance at variable temperatures revealed a multi-carrier transport tendency in the thin films. We determined the carrier densities and mobilities of two majority carriers using the simplified two-carrier model. The electron carriers can be attributed to the Dirac band with a non-trivial Berry phase π, while the hole carriers may originate from surface chemical reaction or unintentional doping during the microfabrication process. It is necessary to encapsulate the $ZrTe_5$ film in an inert or vacuum environment to potentially achieve a substantial improvement in device quality.

Keywords: multi-carrier transport, $ZrTe_5$ film, thickness-dependence, gate-dependence

PACS: 73.50.–h, 73.23.–b, 73.63.–b **DOI:** 10.1088/1674-1056/27/8/087307

1. Introduction

Topological insulators provide a unique platform for exploring novel quantum phases and phenomena, such as the quantum spin Hall (QSH) effect,[1–3] and the quantum anomalous Hall effect,[4,5] etc. $ZrTe_5$ is an orthorhombic layered material, which is predicted to be a 2D topological insulator in a monolayer form.[6] The $ZrTe_5$ bulk system also displays abundant electronic and exotic transport properties, and the topological nature is still unclear, i.e., strong topological insulator,[7] weak topological insulator,[8–10] and Dirac semimetal.[11–13] However, there are significantly fewer experimental studies on $ZrTe_5$ thin films. Moreover, the conversion between three-dimensional (3D) and 2D systems is not fully understood. Since interlayer coupling in $ZrTe_5$ is as weak as graphite, this allows us to reduce the sample's thickness to a monolayer by mechanical exfoliation.[14] More recently, several groups have discovered that the transport properties of $ZrTe_5$, such as the Hall reversal,[15,16] and resistivity-anomaly peak temperature (T_p),[17,18] can be changed by modifying the thickness and temperature. Strong anisotropic transport behavior is also observed in angular geometry devices.[19] The latest angle-resolved photoemission spectroscopy (ARPES) and scanning-tunneling microscopy (STM) results provide strong evidence of the topological protected metallic state at the step edge,[9] which could host the quantum spin Hall state. These phenomena require further transport investigation of the interplay between electrical field, magnetic field, temperature, and thickness, with the objective of gaining a deeper understanding of the still unknown topological nature and resistivity anomaly of thin $ZrTe_5$ films.

In this work, we have systematically performed transport measurements in $ZrTe_5$ thin films, with tuning thickness, temperature, electrical field, and magnetic field. The shifting of T_p and the Hall resistance (R_{xy}) anomaly, which is accompanied by the SdH oscillations, were observed when the thickness was reduced, demonstrating the multi-carrier behavior in the thin films. Using the simplified two-carrier model, we determined the carrier density and mobility of each band. One is a Dirac-like electron band with a high mobility of $\sim 2\times10^4$ $cm^2{\cdot}V^{-1}{\cdot}s^{-1}$ and a low carrier density of $\sim 10^{16}$ cm^{-3}–10^{17} cm^{-3}, which hosts the nontrivial Berry phase clarified by the Landau-Fan diagram analysis of the SdH oscillations.[16] The other is a trivial hole-like band with a low mobility of 10^2 $cm^2{\cdot}V^{-1}{\cdot}s^{-1}$ $\sim 10^3$ $cm^2{\cdot}V^{-1}{\cdot}s^{-1}$ and a high carrier density of 10^{18} cm^{-3} $\sim 10^{19}$ cm^{-3}. Considering the decay of the sample under ambient conditions, this hole band may originate from hole doping by surface chemical reactions. Similar results have also been discussed for several other semimetals, such as Cd_3As_2,[20] WTe_2,[21] $HfTe_5$,[22] $TaAs_2$,[23] and graphite.[24] These observations provide a clue

*Project supported by Guangdong Innovative and Entrepreneurial Research Team Program (Grant No. 2016ZT06D348) and Shenzhen Peacock Program (Grant No. KQTD2016022619565991).

†Corresponding author. E-mail: le.wang@ruc.edu.cn

© 2018 Chinese Physical Society and IOP Publishing Ltd

to understanding the connection between 2D and 3D $ZrTe_5$, and to potentially achieve a substantial improvement in device quality.

2. Experimental methods

A single crystal of $ZrTe_5$ was grown by chemical vapor transport (CVT).[25] The $ZrTe_5$ thin films were prepared by standard mechanical exfoliation of the bulk crystal, then deposited onto silicon substrates with 285-nm SiO_2. The samples were first identified using optical microscopy, then immediately coated with a PMMA film in a glove box filled with argon gas. The exact thickness of the sample was finally measured using Atomic Force Microscopy (model Keysight 5500) after transport measurement. The devices were fabricated by traditional e-beam lithography in a Hall bar geometry. For the thick films, a silicone elastomer polydimethylsiloxane stamp PDMS was used as a media to transfer the film onto prefabricated electrode patterns.[26] Magneto-transport measurements were performed using an Oxford TeslatronPT cryostat with variable temperatures from 1.5 K to 300 K and a magnetic field up to 14 T. The standard lock-in method with a low frequency (17.777 Hz) was used to measure the longitudinal and transverse resistivity. A typical measurement current was 10 nA$\sim$ 1 μA depending on the resistance of the sample. The back gate experiment was performed using a Keithley 2400 source meter.

3. Results and discussion

3.1. Thickness-dependent transport

Figure 1(a) displays the temperature-dependent resistivity of the bulk $ZrTe_5$. The T_p of the bulk sample is 140.1 K, which is a typical value for a $ZrTe_5$ crystal grown by CVT. The ARPES and transport results revealed that T_p is the cutoff point of the temperature-induced Lifshitz transition of the Fermi surface topology.[27,28] The relationship between T_p and the thickness is summarized in Fig. 1(c), while the temperature-dependent resistivity curves of some thin films are plotted in Fig. 1(b). T_p initially decreases with a decrease of the thickness down to 40 nm, then increases with a further reduction of the thickness.[17] It is noteworthy that although the observed tendency indicates a thickness-tuned effect of T_p in Fig. 1(c), the T_ps of thin films (< 40 nm) vary dramatically from 140 K to above 300 K. The conclusion that a highly thickness-tuned transition of the band topology occurs in $ZrTe_5$ films is nonetheless not justified.

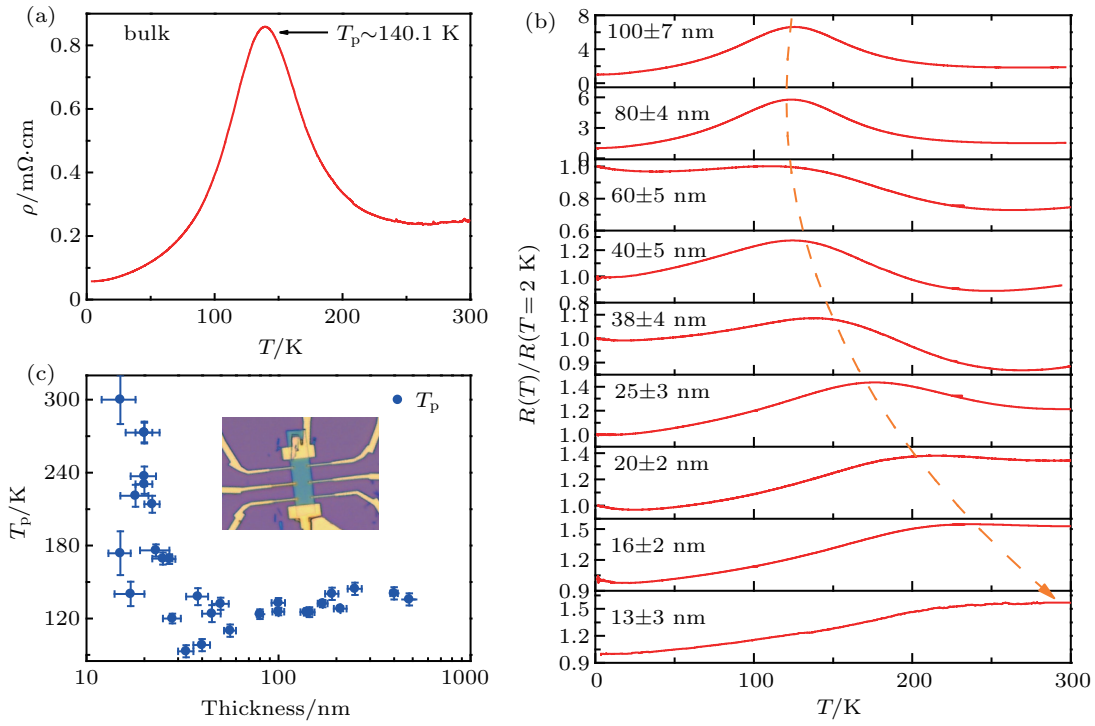


Fig. 1. (color online) Thickness dependence of resistance anomaly temperature in $ZrTe_5$ films. (a) The temperature dependence of the resistivity of bulk $ZrTe_5$. The resistance anomaly temperature (T_p) is approximately 140.1 K. (b) Some selected R–T curves of thickness ranging from 13 nm to 100 nm. (c) Systematic statics of the thickness-dependent T_p transition. The observed tendency is an initial decrease followed by an increase that is largely sample-dependent, indicating the extreme sensitivity of thin samples.

To better understand the thickness-dependent transport property, the Hall resistance of samples with different thicknesses was measured at 1.5 K. As shown in Fig. 2(a), the slopes of the Hall resistance R_{xy} plots for thick samples (> 100 nm) are negative for the entire magnetic field region (14 T) and exhibit nonlinear behavior at a high field. This nonlinear curve indicates the contribution of more than one electron band in the transport. For thin samples (33 nm to 100 nm), the

Hall sign is negative at the low field but becomes positive at a high field. This "Z"-shaped Hall sign reversal implies the participation of a hole-type band.[20] When the thickness is less than 33 nm, the Hall anomaly disappears, and the slopes of the Hall resistance plot are positive, indicating that the hole-type carriers dominate the transport. This Hall resistance transition is consistent with the change of T_p in Fig. 1. However, as shown in Fig. 2(b), this regular behavior is not exhibited in samples with a thickness value between 26 nm and 45 nm. Evidently, a clear difference in the magneto-resistance (MR), as well as the Hall resistance is observed in these samples over a one-week interval. Figure 2(c) illustrates a comparison between the MR and Hall resistance for an 80-nm thick sample. Even though the samples are stored in an argon-filled glove box to minimize surface oxidation, the MR decreases to $\sim 40.4\%$ of the initially measured result, and the slope of the Hall resistance exhibits a larger hole doping value of $\sim 131\%$ relative to the initially measured value.

This significant deviation forces us to consider the effect of decay during the sample preparation process. The decay takes place at the surface, where the activated atoms emerge after being exfoliated from the bulk crystal. These activated atoms can easily react with oxygen, water, and organic solvents during fabrication, leading to giant hole doping at the surface.[29,30] For thick samples ($>$ 100 nm), this effect of surface doping is limited due to the small surface-to-volume ratio. The transport is dominated by electron carriers in the bulk $ZrTe_5$, giving rise to the negative slopes of the Hall resistance. On the contrary, this hole doping at the surface becomes strong enough in thin films to cause the movement of the Fermi level. For samples with a thickness less than 33 nm (see Fig. 2(a)), heavy surface hole-doping carriers dominate the transport, leading to a positive Hall coefficient. For samples with a thickness value between 33 nm and 100 nm, the character of transport is the competitive result of the electron carriers and the surface hole-doping carriers. The level of surface hole doping will influence the transport measurement results, which is confirmed by the time-interval measurement of the MR and Hall resistance as shown in Fig. 2(c).

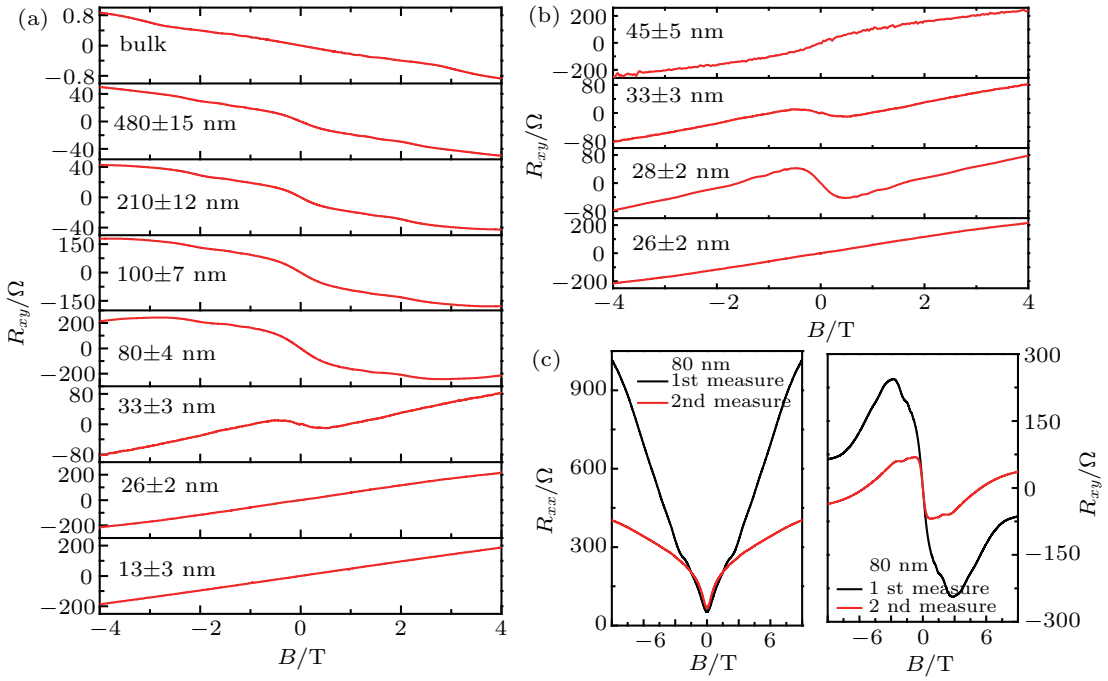


Fig. 2. (color online) (a) Some selected Hall resistance measurements for different thickness values of $ZrTe_5$ films at 1.5 K. The plots display a "suspected" thickness-tuned band transition from electron type to hole type when the thickness is reduced. The Hall anomaly indicates the multi-carrier transport. (b) Some examples of "irregular" thickness-dependent Hall resistance, largely depending on the sample quality. (c) A comparison of the magneto-resistance and Hall resistance of the same sample measured over a one-week interval. The sample was stored in a glove box with an argon atmosphere. Other samples also display a similar decay behavior.

3.2. Magnetic field-dependent transport

Figures 3(a) and 3(b) are the MR and Hall resistance of a 28-nm thick sample in the temperature range from 1.5 K to 200 K, respectively. The MR shows a "V"-shaped curve in a low field accompanied by obvious SdH oscillations below 4 T, and a linear behavior above 4 T. The Hall resistance displays a "Z"-shaped anomalous curve, and changes from negative to positive accompanied by SdH oscillations. This behavior is similar to that of Bi_2Te_3,[31] which is a hallmark of multi-carrier transport in most instances. The electron-to-hole transition disappears between 100 K $\sim$ 140 K, corresponding to the T_p (117 K) of this sample.

To further understand the SdH oscillations, the Landau plotting and effective cyclotron mass fitting were performed. According to the Lifshitz–Kosevich formula,[16,32]

$$\Delta R \propto R_{\rm T} R_{\rm D} R_{\rm S} \cos 2\pi \left(\frac{B_{\rm F}}{B} + \gamma \right), \quad (1)$$

where $R_{\rm T}$, $R_{\rm D}$, and $R_{\rm S}$ are three reducing factors accounting for the phase smearing effect of temperature, scattering, and spin splitting; γ is a phase factor that implies the band singularity, from which Berry's phase of the system is obtained; $B_{\rm F}$ is the slope of the Landau fan diagram; and B is the magnetic field strength. According to the Lifshitz–Onsage quantization rule: $B_{\rm F}/B = N + 1/2 - \Phi_{\rm B}/2\pi - \delta = N + \gamma$, where N is the Landau level index, $\Phi_{\rm B}$ is the Berry phase, and δ is an additional phase shift which has a value of 0 for 2D or $\pm 1/8$ for 3D, and γ is the intercept in the Landau plot. In this case, the peak values are chosen to be the integer indices and the valleys are chosen to be the half-integer indices. For Dirac materials, a $|\gamma|$ value between 0 and 1/8 implies a non-trivial Berry phase π and approximately 1/2 indicates a trivial Berry phase.

Figure 3(c) displays the oscillating amplitude of the resistance after subtracting the high-temperature background, in which Zeeman splitting can be observed.[16] Figure 3(d) displays the Landau–Fan diagram of samples of different thicknesses. All the intercepts have a value close to zero, indicating the nontrivial Berry phase, which has been proven to be a strong characteristic of the Dirac band.[32] Furthermore, the slopes ($B_{\rm F}$), which are directly proportional to the 2D carrier density, decrease when the thickness is reduced, which implies a reduction of the Fermi level due to hole doping. The effective cyclotron mass $m^* \sim 0.057\ m_{\rm e}$ which is fitted by the data in the inset of Fig. 3(d), is of the same order of magnitude as the bulk material $\sim 0.03\ m_{\rm e}$. The 3D carrier density of this band is approximately calculated, resulting in a value of $n_{\rm 3D}^{\rm SdH} \sim (n_{\rm 2D}^{\rm SdH})^{3/2} \sim 5.28 \times 10^{16}$ cm^{-3}, using $g = 2$ (the spin degeneracy of Landau level) and $B_{\rm F} \sim 2.92$ T. The carrier mobility can be estimated from $\mu_{\rm SdH} \cdot B_{\rm on} \sim 1$, leading to the value of 18720 cm$^2 \cdot$V$^{-1} \cdot$s^{-1}, where $B_{\rm on}$ is the onset magnetic field strength of the SdH oscillations. From the aforementioned simplified analysis, the key parameters of the Dirac band are obtained.

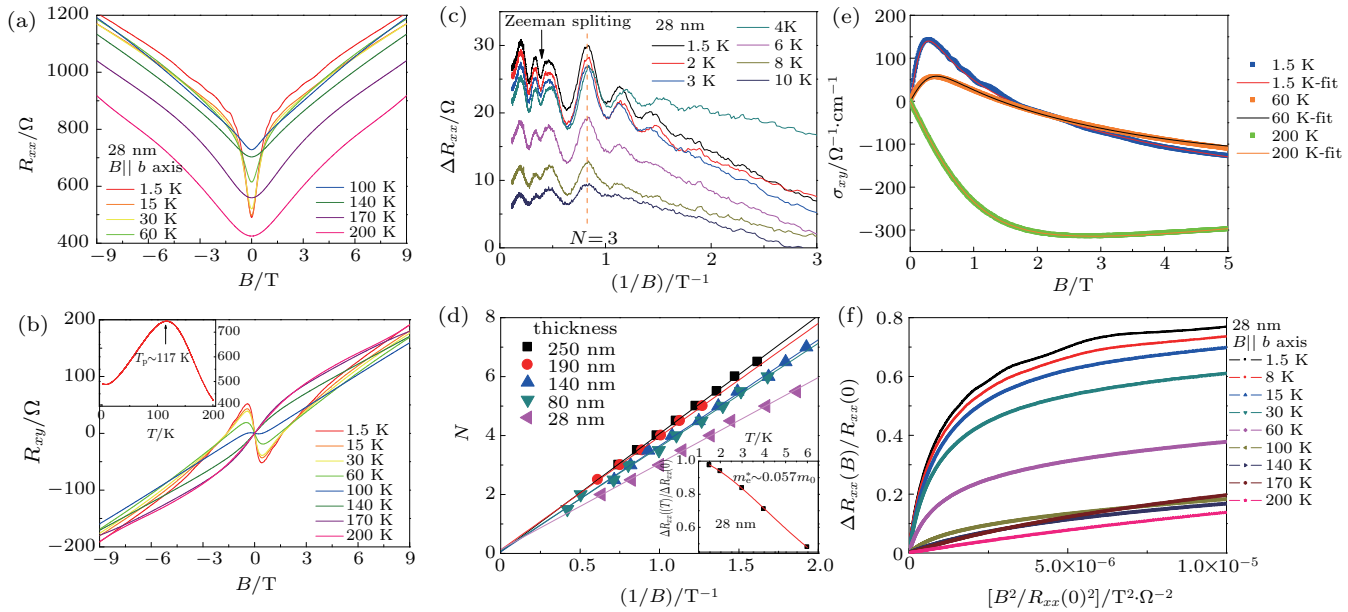


Fig. 3. (color online) Temperature-dependent magneto-transport of the 28-nm $ZrTe_5$ film. (a) and (b) The longitudinal and transverse magneto-resistance of $ZrTe_5$ from 1.5 K to 200 K. Well-defined SdH oscillations are observed in the low field (< 4 T), and the Hall anomaly indicates two types of carriers. (c) The amplitude of the SdH oscillations at different temperatures after subtracting a high temperature background of 15 K, and the Zeeman splitting implies well-resolved Landau levels. (d) The Landau–Fan diagram of $ZrTe_5$ films for different thickness values. The decrease in the slope indicates a reduction in the electron density. The zero intercepts demonstrate the nontrivial Berry phase. The insert represents the fit of the effective cyclotron mass (0.057 $m_{\rm e}$) in the *ac* plane. (e) Two-carrier model fits of the Hall conductivity at 1.5 K, 60 K, and 200 K respectively. (f) The Kohler plot of MR at different temperatures, indicating hole dominating transport above 100 K and multi-carrier transport at low temperature.

We find that the nonlinear property in the Hall resistance is coincident with the multi-carrier transport behavior. For simplification, the carriers are divided into two parts: one is the Dirac band, and the other is regarded as an equivalent hole band with the same scattering time. Thus the standard two-carrier model is applied as,[20,24]

$$\sigma_{xx}^{\rm total} = \frac{\rho_1}{\rho_1^2 + (R_1 B)^2} + \frac{\rho_2}{\rho_2^2 + (R_2 B)^2},$$

$$\sigma_{xy}^{\rm total} = -\frac{R_1 B}{\rho_1^2 + (R_1 B)^2} - \frac{R_2 B}{\rho_2^2 + (R_2 B)^2}. \quad (2)$$

Each band has two parameters: resistivity ρ_i and Hall coefficient $R_i = 1/n_i q_i$, where $q_i = \pm e$ ($i = 1, 2$) is the charge of the carrier. It is necessary to fit σ_{xx} and σ_{xy} simultaneously by adjusting the four parameters independently until the difference between the fitting curves and the experimental data is minimized. We can also determine that the Hall resistance reverses its sign at a critical magnetic field

$B_c = \sqrt{(n_1\mu_1^2 - n_2\mu_2^2)/\mu_1^2\mu_2^2(n_2 - n_1)}$, where μ_1 represents the high mobility Dirac band and μ_2 is the hole band. In the case where $\mu_1 > \mu_2$, the decrease of the electron concentration with increasing temperature will cause the decrease of B_c, consistent with Fig. 3(b). The fitting results are illustrated in Fig. 3(e) at representative 1.5 K, 60 K, and 200 K temperatures. From the best fit, the mobility and carrier density of the Dirac band at 1.5 K are 3.2×10^4 cm^2·V^{-1}·s^{-1} and 5.90×10^{16} cm^{-3} respectively, in agreement with the band parameters obtained from the SdH oscillations. The mobility and carrier density of the hole band are 1018 cm^2·V^{-1}·s^{-1} and 2.25×10^{18} cm^{-3} respectively. In thinner samples, the hole mobility is lowered to $\sim 10^2$ cm^2·V^{-1}·s^{-1} and the carrier density increases to $\sim 10^{19}$ cm^{-3}. It is noteworthy that the two-carrier model is a classical model, which cannot be used in quantum transport with the "V"-shaped MR and the SdH oscillations. However, the good description of the transport behavior in this case demonstrates the validity of the two-carrier model to some degree.

To reveal two-carrier transport in $ZrTe_5$ thin films, we use Kohler's plots[33,34] with $\Delta R_{xx}(B)/R_{xx}(0) \sim (B/R_{xx}(0))^2$ for the classical B^2 dependence of MR, as shown in Fig. 3(f). If there is one type of carrier with the same scattering time everywhere at the Fermi surface, the temperature-dependent Kohler plots of the MR curves could overlap each other. At a temperature above 100 K, the collapsed curves are indicative of hole-dominating transport, although there are two types of holes. At a low temperature, the curves separate from each other because of the increase in the number of Dirac electrons with high mobility.

3.3. Field-effect transport

The gate-dependent longitudinal conductivity of thin films without an external magnetic field was also investigated. For thicker samples (> 30 nm), gate tuned doping is limited because of the Thomas-Fermi dielectric screening.[35,36] The gate voltage can only modulate about 5% ~ 20% of the original resistance without doping. For thin samples, the gate effect becomes larger, and most of the samples show p-type curves instead of an ambipolar behavior. In thin films with less decay, it is possible to observe the ambipolar behavior. Figure 4(a) illustrates the transfer curves of a 15 nm thick sample from 3.6 K to 270 K. The inset represents the typical gate-tuned longitudinal conductivity at 3.6 K, in which a minimum of conductivity (V_D) at $V_g = 60$ V is observed. The minimum point indicates the transition from the p-type to n-type. It should be noted that this transition point is different from the neutral point in semiconductors or graphene.[37,38] We believe that this is a comprehensive result of the contributions of the two carrier densities and mobilities, which is exceptional evidence of the electron-hole asymmetric system. This minimum point shifts toward the positive gate voltage with an increase of the temperature, and disappears above 70 K continued by the p-type behavior. This transform may be caused by the downward temperature-induced Fermi level shift from the conduction band to the valence band.

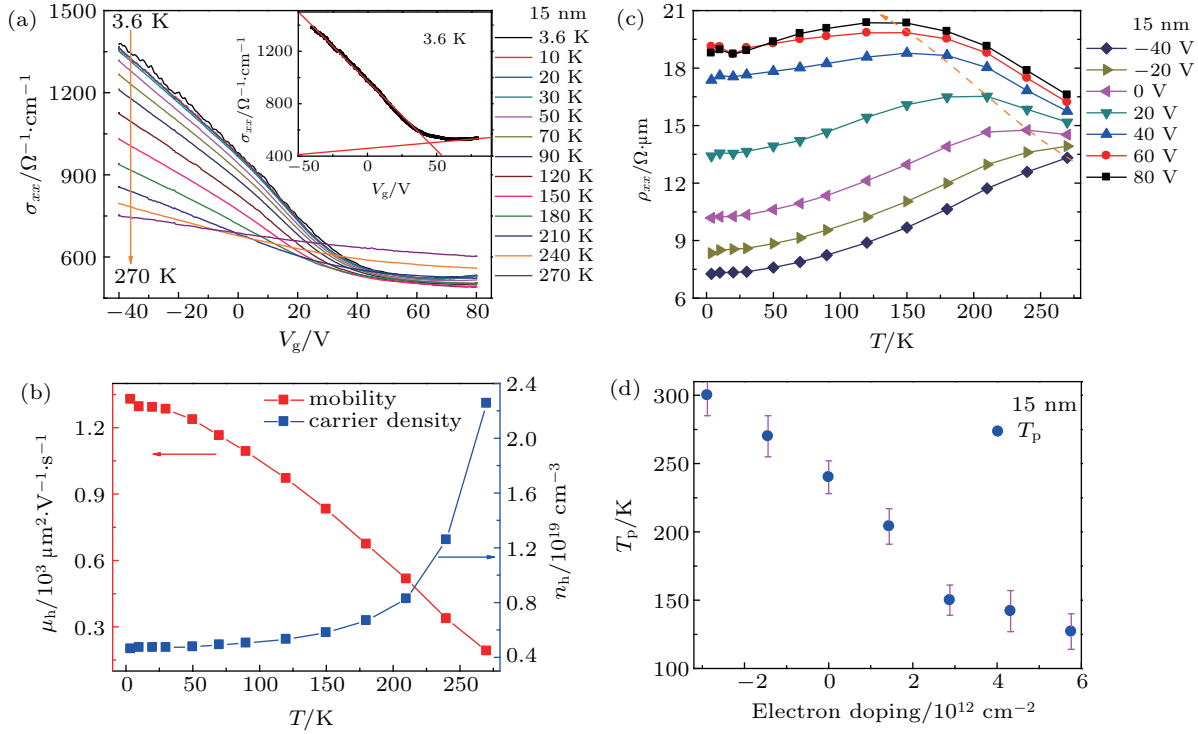


Fig. 4. (color online) (a) The gate voltage modulated longitudinal conductivity of the 15-nm $ZrTe_5$ films at different temperatures. The results show a peak near 60 V at 3.6 K. (b) The field effect mobility of the dominated hole type carriers and the carrier density as estimated using the Drude model. (c) The corresponding temperature-dependent longitudinal resistivity at different voltages displays the movement of T_p. (d) T_p moves to a lower temperature with an increase in electrons doping, indicating the easy modulation due to the external doping level.

The field-effect mobility $\mu_{\rm FE}$ in the linear region of the transfer characteristics can be determined using the following formula,[39]

$$\mu_{\rm FE} = \frac{\partial \sigma_{xx}}{\partial V_g} \frac{dt}{\varepsilon_0 \varepsilon_{ox}}, \tag{3}$$

where d and t are the thickness of the film and the SiO_2 dielectric layer, respectively, and $\varepsilon_{ox} = 3.9$ is the dielectric constant of SiO_2. Using the classical Drude model $\sigma_{xx} = ne\mu_{\rm FE}$, the carrier density of the dominating p-type carrier can be roughly estimated, as shown in Fig. 4(b). This estimation is reasonable because the hole carrier density is 2∼ 3 orders larger than the electron carrier density, deduced by two-carrier fitting in the previous section. When the temperature changes from 270 K to 3.6 K, the hole mobility increases from 192 $cm^2 \cdot V^{-1} \cdot s^{-1}$ to 1330 $cm^2 \cdot V^{-1} \cdot s^{-1}$, and the carrier density decreases from 2.3×10^{19} cm^{-3} to 4.1×10^{18} cm^{-3}. The values obtained for these two parameters are consistent with the results of the two-carrier model fitting.

Figure 4(c) displays the temperature-dependent longitudinal resistivity for different applied gate voltages, extracted from the transfer curves in Fig. 4(a). The resistivity anomaly points are summarized in Fig. 4(d), in which the $T_{\rm p}$ obviously changes from above 270 K down to 120 K when electron doping is increased. This result provides a good explanation for the dramatic variation of the $T_{\rm p}$s in thin films shown in Fig. 1(c). When the sample gets thinner, the surface-to-volume ratio becomes larger, and hole doping will increase if the exposing time is increased. Samples of similar thickness may experience heavier or lighter doping, which causes $T_{\rm p}$ to change.

3.4. Magneto-resistance with gating effect

Figure 5(a) shows the gate-tunable MR behaviors of the 80-nm thick sample at 1.5 K. The magnetic field is parallel to the b axis. The "V"-shaped MR and the "Z"-shaped Hall resistance for different gate voltages demonstrate the two-carrier transport character. As shown in Fig. 5(b), all the Landau-plotting curves are overlapped in the same fitting line. Although different gate voltages are applied, the same Landau levels of the SdH oscillations are still located in the same magnetic field. We believe that most of the doped carriers go into the p-type band of the surface, instead of doping the Dirac band. This result corresponds to the fitting result of the two-carrier model, and indicates that the carrier density and mobility of the Dirac band hardly change, while the hole-type carrier density decreases when a larger gate voltage is applied.

Finally, we study the gate effect of $ZrTe_5$ devices at different magnetic field strengths.[19] As shown in Fig. 5(c) and Fig. 5(d), the transfer curves of a 31-nm thick device exhibit the monotonous p-type behavior in all the field ranges, indicating hole dominating transport. The transfer mobility is approximately 690 $cm^2 \cdot V^{-1} \cdot s^{-1}$, which was validated using the fitting value of 770 $cm^2 \cdot V^{-1} \cdot s^{-1}$ from the Hall measurement, as shown in the inset figure. The small increase of the Hall resistance implies a decrease of the population of the hole (seen in Fig. 5(d)). No SdH oscillations are observed in this thin sample. This may be due to the low mobility and high carrier density in the heavy hole-doping sample.

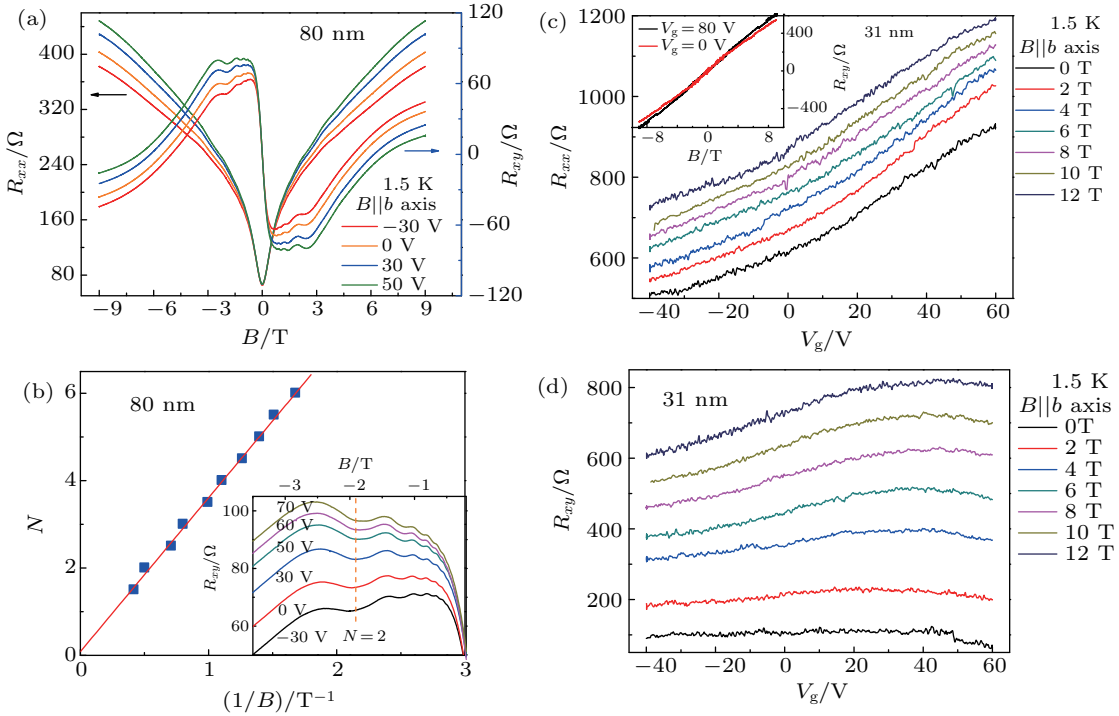


Fig. 5. (color online) The gate voltage modulated magnetotransport at 1.5 K. (a) The MR and Hall resistance of the 80-nm sample. (b) The Landau plot of the SdH oscillations, indicating the nontrivial Berry phase. The inset represents the Landau levels at different gate voltages. (c) and (d) The p-type gate effect of MR and the Hall resistance at different magnetic field strengths for the 31-nm sample.

4. Conclusions

In summary, we have systematically performed low-temperature magnetotransport measurements to investigate thickness-dependence, temperature-tuning, and gate-modulation in $ZrTe_5$ films. We determined that T_p increases as the thickness of the $ZrTe_5$ is reduced. However, the T_p values are irregular and exhibit a large sample dependence, especially below 40 nm. Combining the SdH oscillations and Hall measurements, we determined the carrier densities and mobilities using two-carrier model fitting: one electron band hosts a high mobility of $\sim 2\times10^4$ $cm^2{\cdot}V^{-1}{\cdot}s^{-1}$ and a low carrier density of $\sim 10^{16}$ cm^{-3}–10^{17} cm^{-3}; the other hole band has a low mobility of 10^2 $cm^2{\cdot}V^{-1}{\cdot}s^{-1}$ $\sim 10^3$ $cm^2{\cdot}V^{-1}{\cdot}s^{-1}$ and a high carrier density of 10^{18} cm^{-3} $\sim 10^{19}$ cm^{-3}. Considering the effect of decay on the sample surface, we propose that the multi-carrier transport property is induced by the coexistence of the Dirac-like electron band with a nontrivial Berry's phase, and the trivial hole-like band from unintended surface chemical reactions. We anticipate that these results will be helpful in attempting to understand the conversion between a bulk system to a thin film. A stricter fabrication process is required using a uniform insulating substrate (i.e., hexagonal boron-nitride) as the capping layer, which may facilitate a reliable way to study the QSH effect and topological phase transitions in $ZrTe_5$ films.

References

[1] Murakami S, Nagaosa N and Zhang S C 2003 *Science* **301** 1348
[2] Konig M, Wiedmann S, Brüne C, Roth A, Buhmann H, Molenkamp L W, Qi X L and Zhang S C 2007 *Science* **318** 766
[3] Tang S, Zhang C, Wong D, Pedramrazi Z, Tsai H Z, Jia C, Moritz B, Claassen M, Ryu H and Kahn S 2017 *Nat. Phys.* **13** 683
[4] Chang C Z, Zhang J, Feng X, Shen J, Zhang Z, Guo M, Li K, Ou Y, Wei P and Wang L L 2013 *Science* **340** 167
[5] Feng X, Feng Y, Wang J, Ou Y, Hao Z, Liu C, Zhang Z, Zhang L, Lin C and Liao J 2016 *Adv. Mater.* **28** 6386
[6] Weng H M, Dai X and Fang Z 2014 *Phys. Rev. X* **4** 011002
[7] Manzoni G, Gragnaniello L, Autes G, Kuhn T, Sterzi A, Cilento F, Zacchigna M, Enenkel V, Vobornik I, Barba L, Bisti F, Bugnon P, Magrez A, Strocov V N, Berger H, Yazyev O V, Fonin M, Parmigiani F and Crepaldi A 2016 *Phys. Rev. Lett.* **117** 237601
[8] Li X B, Huang W K, Lv Y, Zhang K W, Yang C L, Zhang B B, Chen Y B, Yao S H, Zhou J, Lu M H, Sheng L, Li S C, Jia J F, Xue Q K, Chen Y F and Xing D Y 2016 *Phys. Rev. Lett.* **116** 176803
[9] Wu R, Ma J Z, Nie S M, Zhao L X, Huang X, Yin J X, Fu B B, Richard P, Chen G F, Fang Z, Dai X, Weng H M, Qian T, Ding H and Pan S H 2016 *Phys. Rev. X* **6** 021017
[10] Moreschini L, Johannsen J C, Berger H, Denlinger J, Jozwiack C, Rotenberg E, Kim K S, Bostwick A and Grioni M 2016 *Phys. Rev. B* **94** 081101
[11] Li Q, Kharzeev D E, Zhang C, Huang Y, Pletikosić I, Fedorov A V, Zhong R D, Schneeloch J A, Gu G D and Valla T 2016 *Nat. Phys.* **12** 550
[12] Zheng G, Lu J, Zhu X, Ning W, Han Y, Zhang H, Zhang J, Xi C, Yang J, Du H, Yang K, Zhang Y and Tian M 2016 *Phys. Rev. B* **93** 115414
[13] Chen R Y, Chen Z G, Song X Y, Schneeloch J A, Gu G D, Wang F and Wang N L 2015 *Phys. Rev. Lett.* **115** 176404
[14] Geim A K and Grigorieva I V 2013 *Nature* **499** 419
[15] Liang T, Lin J, Gibson Q, Kushwaha S, Liu M, Wang W, Xiong H, Sobota J A, Hashimoto M and Kirchmann P S 2018 *Nat. Phys.* **14** 451
[16] Liu Y, Yuan X, Zhang C, Jin Z, Narayan A, Luo C, Chen Z, Yang L, Zou J, Wu X, Sanvito S, Xia Z, Li L, Wang Z and Xiu F 2016 *Nat. Commun.* **7** 12516
[17] Lu J, Zheng G, Zhu X, Ning W, Zhang H, Yang J, Du H, Yang K, Lu H and Zhang Y 2017 *Phys. Rev. B* **95** 125135
[18] Niu J J, Wang J Y, He Z J, Zhang C L, Li X Q, Cai T C, Ma X M, Jia S, Yu D P and Wu X S 2017 *Phys. Rev. B* **95** 035420
[19] Qiu G, Du Y, Charnas A, Zhou H, Jin S, Luo Z, Zemlyanov D Y, Xu X, Cheng G J and Ye P D 2016 *Nano Lett.* **16** 7364
[20] Li C Z, Li J G, Wang L X, Zhang L, Zhang J M, Yu D and Liao Z M 2016 *ACS Nano* **10** 6020
[21] Wang Y, Wang K, Reuttrobey J, Paglione J and Fuhrer M S 2016 *Phys. Rev. B* **93** 121108
[22] Zhao L X, Huang X C, Long Y J, Chen D, Liang H, Yang Z H, Xue M Q, Ren Z A, Weng H M, Fang Z, Dai X and Chen G F 2017 *Chin. Phys. Lett.* **34** 037102
[23] Wu D, Liao J, Yi W, Wang X, Li P, Weng H, Shi Y, Li Y, Luo J and Dai X 2016 *Appl. Phys. Lett.* **108** 042105
[24] Du X, Tsai S W, Maslov D L and Hebard A F 2005 *Phys. Rev. Lett.* **94** 166601
[25] Shahi P, Singh D J, Sun J P, Zhao L X, Chen G F, Yan J Q, Mandrus D G and Cheng J G 2016 *Phys. Rev. X* **8** 021055
[26] Xi X, Wang Z, Zhao W, Park J H, Law K T, Berger H, Forró L, Shan J and Mak K F 2016 *Nat. Phys.* **12** 139
[27] Zhang Y, Wang C, Yu L, Liu G, Liang A, Huang J, Nie S, Sun X, Zhang Y, Shen B, Liu J, Weng H, Zhao L, Chen G, Jia X, Hu C, Ding Y, Zhao W, Gao Q, Li C, He S, Zhao L, Zhang F, Zhang S, Yang F, Wang Z, Peng Q, Dai X, Fang Z, Xu Z, Chen C and Zhou X J 2017 *Nat. Commun.* **8** 15512
[28] Wu Y, Jo N H, Ochi M, Huang L, Mou D, Bud'Ko S L, Canfield P C, Trivedi N, Arita R and Kaminski A 2015 *Phys. Rev. Lett.* **115** 166602
[29] Huang S M, Huang C Y, Huang S J, Hsu C, Yu S H, Chou M, Wadekar P V, Chen Y S and Tu L W 2017 *J. Appl. Phys.* **121** 054311
[30] Thomas C R, Vallon M K, Frith M G, Sezen H, Kushwaha S K, Cava R J, Schwartz J and Bernasek S L 2016 *Chem. Mater.* **28** 35
[31] Qu D X, Hor Y S, Xiong J, Cava R J and Ong N P 2010 *Science* **329** 821
[32] Murakawa H, Bahramy M S, Tokunaga M, Kohama Y, Bell C, Kaneko Y, Nagaosa N, Hwang H Y and Tokura Y 2013 *Science* **342** 1490
[33] Ishiwata S, Shiomi Y, Lee J S, Bahramy M S, Suzuki T, Uchida M, Arita R, Taguchi Y and Tokura Y 2013 *Nat. Mater.* **12** 512
[34] Husmann A, Betts J B, Boebinger G S, Migliori A, Rosenbaum T F and Saboungi M L 2002 *Nature* **417** 421
[35] Resta R 1977 *Phys. Rev. B* **16** 2717
[36] Newns D M 1969 *J. Chem. Phys.* **50** 4572
[37] Zhang Y, Tan Y W, Stormer H L and Kim P 2005 *Nature* **438** 201
[38] Li L, Yang F, Ye G J, Zhang Z, Zhu Z, Lou W, Zhou X, Li L, Watanabe K and Taniguchi T 2016 *Nat. Nanotechnol.* **11** 593
[39] Li L, Yu Y, Ye G J, Ge Q, Ou X, Wu H, Feng D, Chen X H and Zhang Y 2014 *Nat. Nanotechnol.* **9** 372